JOURNAL OF GEOPHYSICAL RESEARCH, VOL. 113, C01002, doi:10.1029/2006JC004057, 2008

Resonant excitation of the quasi-decadal oscillation by the 11-year signal in the Sun's irradiance

Warren B. White[1] and Zengyu Liu[2]

Received 14 December 2006; revised 23 February 2007; accepted 14 May 2007; published 4 January 2008.

[1] The quasidecadal oscillation (QDO) of 9- to 13-year period in the Earth's climate system has been found governed by a delayed action oscillator (DAO) mechanism in the tropical Pacific Ocean similar to that governing the El Niño–Southern Oscillation (ENSO) of 3- to 5-year period. It also fluctuated in phase with the ~11-year-period signal in the Sun's total irradiance throughout the twentieth century. In earlier attempts to explain this association, a conceptual ocean-atmosphere coupled model of the DAO mechanism in the tropical Pacific Basin was driven by 11-year-period solar forcing, producing a QDO that was in damped resonance with the solar forcing. In the present study, we likewise force a fully coupled ocean-atmosphere general circulation model (i.e., Fast Ocean-Atmosphere Model (FOAM)) of Jacob et al. (2001), adding an 11-year-period cosine signal of amplitude ~2.0 W m^{-2} to the solar constant in the model. In the presence of this 11-year-period solar forcing the FOAM simulates both the ENSO and the QDO, while in its absence the FOAM simulates only the ENSO. We find the model QDO governed by a tropical DAO mechanism with patterns and evolution similar to those observed. We find its warm phase lagging peak solar forcing by ~1–3 years, as observed and consistent with damped-resonant excitation of the tropical DAO of the QDO by the 11-year-period solar forcing in the earlier conceptual model.

Citation: White, W. B., and Z. Liu (2008), Resonant excitation of the quasi-decadal oscillation by the 11-year signal in the Sun's irradiance, *J. Geophys. Res.*, *113*, C01002, doi:10.1029/2006JC004057.

1. Introduction

[2] The quasidecadal oscillation (QDO) of 9- to 13-year period is one of seven narrowband signals ranging in period from 2 to 20 years observed in global patterns of sea surface temperature (SST) and sea level pressure (SLP) during the late nineteenth and twentieth Century [*Allan*, 2000; *White and Tourre*, 2003]. The QDO is characterized by global patterns of SST and SLP variability similar to those characterizing the four narrowband El Niño–Southern Oscillation (ENSO) signals ranging in period from 3 to 7 years, and the quasibiennial oscillation (QBO) centered near 2.3-year period, while bearing less resemblance to the interdecadal oscillation (IDO) near 17-year period [*Allan*, 2000; *Tourre et al.*, 2001; *White and Tourre*, 2003, *White et al.*, 2003b]. The QDO is also associated with global-average temperature variability in the upper ocean ranging in magnitude over ~0.1°C, dominated by the tropical global average from 20°S to 20°N [*White et al.*, 2003a]. *Allan et al.* [2003] found the constructive interference of the QBO, the 3- to 7-year-period ENSO signals, and the QDO explaining the occurrence of 'protracted' El Niño and La Niño episodes during the twentieth century, as observed in a case study of the 'protracted' 1992 El Niño episode [*White et al.*, 2003b].

[3] An important issue is the source of these seven signals in the global ocean/atmosphere system. While a more broadband ENSO of 3- to 5-year period has been generally shown in modeling studies to be stochastically forced in the tropical Pacific Ocean [e.g., *Philander*, 1990], no such simulation has been made of the narrowband QBO, ENSO, and QDO signals. This is particularly true of the QDO, whose global SST and SLP patterns of variability, and associated tropical warming, have been found fluctuating in phase with the ~11-year-period signal in the Sun's total irradiance during the twentieth century [*White et al.*, 1997, 1998; *Allan*, 2000; *White and Tourre*, 2003].

[4] In an attempt to understand the thermodynamics of this associated tropical warming, *White et al.* [1998] examined the transient Stefan-Boltzmann (S-B) radiation model for the response of the tropical upper ocean to the surface radiative forcing by the 11-year-period signal in the Sun's total irradiance. They found the corresponding surface radiative forcing (0.2–0.3 W m^{-2}) too weak by factors of 2 to 3 to explain the magnitude of the quasidecadal diabatic heat storage tendency averaged across the tropical global ocean, and they found the phase lag (i.e., ~30°) much less than the 90° phase lag simulated in the transient S-B radiation model. Subsequently, *White et al.* [2003a] diagnosed the thermal budget of the tropical global-average diabatic heat storage variability in the upper ocean associ-

[1]Scripps Institution of Oceanography, University of California, San Diego, La Jolla, California, USA.
[2]Center for Climate Research, Gaylord Nelson Institute for Environmental Studies, University of Wisconsin-Madison, Madison, Wisconsin, USA.

0148-0227/08/2006JC004057$09.00

ated with the QDO, finding its tendency driven not by variable solar forcing but by variable sensible-plus-latent heat flux of ~0.5 W m^{-2} from the lower troposphere.

[5] This led *White* [2006] to diagnose the thermal budget of tropical global-average temperature variability in the atmosphere associated with the QDO. First of all, he found the lower troposphere temperature 0.1°–0.2°C warmer than the underlying sea surface temperature of ~0.1°C across most of the tropical ocean prior to peak solar forcing. Second, he found this tropical lower troposphere temperature variability of ~0.2°C driven by anomalous vertical thermal advection; that is, the mean Hadley circulation operated on anomalous changes in lapse rate due to much larger temperature variability in the lower stratosphere (~1.0°C) and upper troposphere (~0.7°C). *White* [2006] found quasidecadal temperature variability in the lower stratosphere driven principally by the absorption of the Sun's variable UV radiation by mean ozone concentration, with its relatively large magnitude occurring because the ~11-year-period UV component of the total solar irradiance fluctuated 2–3% about the mean UV component, while the ~11-year-period total solar irradiance fluctuated <0.1% about the mean total irradiance [*Lean et al.*, 1995b]. *White* [2006] found the subsequent ~11-year-period warming tendency in the lower troposphere matched by the downward sensible-plus-latent heat flux anomaly across the air-sea interface, with magnitude and phase as observed [*White et al.*, 2003a], thereby explaining the tropical global-average diabatic heat storage tendency in the upper ocean. These thermodynamics also explained the greater-than-one climate sensitivity of the Earth's surface to the 11-year-period solar total irradiance variability [*Reid*, 1991; *White et al.*, 1998; *Douglass and Clader*, 2002].

[6] Here we focus on the source of the QDO itself (i.e., its patterns and evolution in the tropical Pacific Basin), which has been observed governed by the same DAO mechanism responsible for the ENSO in the tropical Pacific Basin [*White et al.*, 2003b]. Earlier, *Graham et al.* [1990] determined theoretically that quasidecadal variability was as much a natural mode of variability as interannual variability in the DAO mechanism for ENSO in the tropical Pacific Basin [*Zebiak and Cane*, 1987; *Graham and White*, 1988; *Schopf and Suarez*, 1988]. However, this quasidecadal variability depended on the delayed negative feedback onto equatorial SST variability from off-equatorial Rossby waves farther poleward (12° to 18° latitude) than observed for ENSO (5° to 12° latitude). *Graham et al.* [1990] were unable to explain why such a quasidecadal signal would be preferentially excited above the background spectrum of noise. Nor could *Capotondi and Alexander* [2001] who were first to observe quasidecadal baroclinic Rossby waves in the latitude domain 10°N–20°N in the North Pacific Ocean.

[7] To begin answering this question, *White et al.* [2001] drove the conceptual coupled model of *Graham et al.* [1990] for the generalized DAO mechanism in the tropical Pacific Basin with the 11-year-period solar forcing. This model yielded a quasidecadal narrowband signal (i.e., the QDO) rising significantly above the background spectrum of noise, with magnitude comparable to that of the ENSO, and indeed depending on the delayed negative feedback from Rossby waves farther away from the equator between 12° and 18° latitude. Because the amplitude of the model QDO was an order of magnitude larger than the S-B response, *White et al.* [2001] proposed that the QDO was in damped resonance with the 11-year period solar forcing.

[8] In the present study, we test this damped-resonant excitation hypothesis for the QDO by driving a fully coupled ocean-atmosphere-terrestrial general circulation model, the Fast Ocean-Atmosphere Model (FOAM) of *Jacob et al.* [2001], with an idealized 11-year-period signal in the Sun's total irradiance represented by an cosine wave of amplitude 2.0 W m^{-2} added to the mean solar irradiance of ~1367 W m^{-2}. This idealized 11-year-period signal in the Sun's total irradiance (i.e., ~0.1% of the mean) yielded radiative forcing of the top of the tropical atmosphere (i.e., averaged around the globe and taking into account the albedo) with an amplitude of ~0.5 W m^{-2} [*White et al.*, 1998]. This estimate is comparable to the radiative forcing by the Sun's 11-year-period signal in UV irradiance found heating-period the tropical lower stratosphere [*White*, 2006] and to the subsequent variable tropical global-average sensible-plus-latent heat flux into the upper ocean of ~0.5 W m^{-1}. Here, in the present FOAM simulation, we have applied this solar forcing directly to the model troposphere and upper ocean, the model lacking the capacity for the lower stratospheric ozone absorption of the much larger percentage variability of the Sun's UV radiative forcing [*Lean et al.*, 1995b].

[9] We find in the absence of the 11-year-period solar forcing that the FOAM does not simulate the QDO. Rather, in this control integration the FOAM simulates an ENSO of 2.9- to 4.5-year periodicity with global patterns and evolution similar to those observed [*Liu et al.*, 2000]. This is viewed as a necessary condition for the QDO to be resonantly excited by the 11-year-period solar forcing in the FOAM [*White et al.*, 2001]; that is, the FOAM must be capable of simulating the tropical DAO mechanism responsible for the ENSO in the Pacific Basin [*White et al.*, 2003b] in order to have the potential for simulating the QDO. Remember, the QDO is hypothesized to be a latent mode of the tropical Pacific DAO mechanism, able to be excited only when the 11-year-period solar forcing is applied [*White et al.*, 2001]. Thus we were not surprised to find that when the 11-year-period solar forcing was used to drive the FOAM, it excited the QDO signal and yielded patterns and evolution in the tropical Pacific Basin similar to those observed [*White et al.*, 2003b].

2. Data and Methods

[10] We use the FOAM in this modeling study [*Jacob et al.*, 2001], integrating it over 350 years without flux adjustment. The atmosphere general circulation model (AGCM) component uses the parallel CCM2 dynamics (PCCM3) [*Drake et al.*, 1995] and CCM3 physics, and has a horizontal resolution of R15 (7.5°longitude by 4.5° latitude) and 18 vertical sigma levels. The ocean general circulation model (OGCM) component has a horizontal resolution of 2.8° longitude by 1.4° latitude and 32 vertical levels in z coordinate. Without any flux adjustment, FOAM has been integrated for many hundreds of years with no apparent climate drift [*Liu and Yang*, 2003].

[11] FOAM has managed to capture most of the major features in the observed global climatology, as in many state-of-the-art climate models [*Liu et al.*, 2003]. It also produces reasonable climate variability, including the patterns and evolution of the ENSO [*Liu et al.*, 2000], Pacific decadal variability [*Wu et al.*, 2003], tropical Atlantic variability [*Liu et al.*, 2004], and North Atlantic variability [*Wu and Liu*, 2005], although the magnitude is usually weaker than observed. *Zhong* [2004] already conducted a preliminary examination of the FOAM response to this 11-year-period signal in the Sun's total irradiance, finding the global-average surface air temperature fluctuating $\pm 0.1^{\circ}$C, the maximum lagging peak solar forcing by $\sim$1 year, similar to that observed [*White et al.*, 1997, 1998]. Furthermore, the zonal-average upper ocean temperature response to solar forcing (i.e., averaged vertically from the sea surface to the top of the main pycnocline) was largest in the tropics and decreased toward the extratropics, as observed [*White et al.*, 1998].

[12] We examine the response of the FOAM [*Jacob et al.*, 2001] to an idealized 11-year-period signal in the Sun's total irradiance, performing an experiment in which the Sun's total irradiance normal to the Earth of 1367 W m^{-2} is augmented by an 11-year period cosine wave with amplitude of 2.0 W m^{-2}. The corresponding solar radiative forcing averaged over the globe is a factor of $\sim$5 less than this ($\sim$0.4 W m^{-2}), while that averaged across the tropics from 20°S to 20°N is a factor of $\sim$4 less than this ($\sim$0.5 W m^{-2}) [*Lean et al.*, 1995a; *White et al.*, 1997; *White*, 2006]. These estimates of tropical solar radiative forcing are similar to the indirect forcing of the tropical upper ocean by variable sensible-plus-latent heat flux ($\sim$0.5 W m^{-2}) stemming from the average warming across the tropical lower troposphere by the $\sim$11-year-period signal in the Sun's UV irradiance absorbed by ozone in the tropical lower stratosphere [*White*, 2006]. The model experiment is started from an equilibrium state provided by the long-term stable control integration and subsequently integrated for 450 years. All of the model integrations examined here are based on model data from the last 350 years. For both the experiment and control simulations, the CO_2 concentration was set to present-day level of 350 ppm. No volcanic aerosol forcing was imposed.

[13] This FOAM experiment is not without its deficiencies. The FOAM climatology exhibits an unrealistic double ITCZ along the entire tropical global ocean [*Liu et al.*, 2004] and a Cold Tongue in the eastern equatorial Pacific Ocean that extends too far into the western ocean [*Liu et al.*, 2000]. Furthermore, the solar-forced FOAM experiment is vastly oversimplified; i.e., representing the $\sim$11-year-period signal in the Sun's total irradiance with cosine variability of uniform amplitude, and assuming the percentage changes to be unrealistically uniform across the Sun's UV, visible, and IR irradiance spectrum [*Lean et al.*, 1995a, 1995b]. However, despite these difficulties, the FOAM simulated a model QDO with a magnitude that rivals that of the model ENSO, and with patterns and evolution in the Pacific Basin similar to those observed [*White et al.*, 2003b].

[14] In the present study, we examine the evolution of the tropical DAO mechanism responsible for the ENSO and QDO in the Pacific Basin of FOAM by conducting an analysis similar to that used to reveal the tropical DAO mechanism of these same observed signals in the Pacific Basin [*White et al.*, 2003b]. This analysis utilizes five variables taken from the middle 100 years (i.e., from year 150 to year 250) of the 350-year FOAM simulation for both the control and solar-forced integrations. These five variables are the monthly zonal surface wind (ZSW), meridional surface wind (MSW), wind stress curl (WSC), sea surface temperature (SST), and the heat storage (HS) over the upper 500 m of ocean, the latter variable representing fluctuations in the main pycnocline of the component OGCM which in observed data was given by the depth of the 18°C isotherm [*White et al.*, 2003b]. Here we combine ZSW and MSW variability into a vector representation of the surface wind (SW) variability.

[15] The analysis begins by comparing observed and model local fractional variance spectra from multitaper method-singular value decomposition (MTM-SVD) methodology [*Mann and Park*, 1999], applying the latter to simulated monthly SST variability over the global ocean by the FOAM during three 100-year records from 50 to 350 years of the model integration (under solar forcing) and to observed SST variability from the HadISST1 data set over the 100-year record from 1900 to 2000 [*Rayner et al.*, 2003]. This comparison of the MTM-SVD local fractional variance spectra finds the model ENSO and narrowband QDO at frequencies similar to those observed. Subsequently, we compare the spatial phase sequences of the dominant complex SVD modes of the ENSO and QDO from the FOAM and from observed SST variability over the global ocean. These spatial phase sequences consist of 7 maps that display 180° of the phase (1/2 cycle) of ENSO and QDO variability, each map extending longitudinally around the globe from 40°S to 40°N.

[16] In order to reveal the tropical DAO mechanism governing both the model ENSO and QDO in the solar-forced FOAM, we band-pass filter the time sequences of monthly model anomalies from the middle 100-year record (i.e., from 150 to 250 years of the 350-year integration) using a period admittance window with half-power points at 3- and 5-year period (i.e., centered near 4-year period) for the model ENSO signal, and 9- and 13-year period (centered near 11-year period) for the model QDO signal [*Kaylor*, 1977]. Since the filter response function of *Kaylor* [1977] is flat, with steep sides and negligible side lobes, the narrowband QDO near 11-year period is effectively isolated from the narrowband ENSO near 4-year period. For the 100-year record, band-pass filtering yields $\sim$27 and $\sim$9 cycles of the ENSO and QDO variability, respectively, yielding approximately $\sim$54 and $\sim$18 effective temporal degrees of freedom [*Snedecor and Cochran*, 1980].

[17] To illustrate the spatiotemporal evolution of the ENSO and QDO in the FOAM, we follow the methodology of *White et al.* [2003b] by applying the extended empirical orthogonal function (EEOF) analysis [*Weare and Nasstrom*, 1982] to filtered SST, ZSW, MSW, WSC, and HS anomalies over the Pacific Ocean from 40°S to 40°N for the 100 years from year 150 to year 250 in the 350-year FOAM integration, over an epoch twice that of the observed variables (1955–1999) analyzed by *White et al.* [2003b]. In EEOF analysis, each map of anomalous variability in the 100-year time sequence is replaced by a sequence of 7 temporal-lag maps. These lag sequences yield the evolution of variability over $\sim$1/2 cycle of each signal, with the 7 temporal-lag

maps resolving the 1/2 cycle in increments of ~30° of phase. Thus EEOF analysis yields time-lagged spatial sequences that are modified by corresponding time sequences of amplitudes. In order to compare the EEOF lag sequences of one variable with that of another, we normalize them, giving them unit variance over the Pacific Basin, with magnitude carried by the time sequence of the amplitudes. The last map in each lag sequence can be multiplied by the time sequence of amplitudes to reveal its contribution to the original time sequence of anomaly maps. Here we display the ~1/2 cycle going from the tropical cool phase to the tropical warm phase of the model ENSO and QDO. We conduct this EEOF analysis on the different variables independently so as not to artificially impose covariability.

3. Local Fractional Variance Spectra of the Observed and Model SST Variability

[18] The local fractional variance spectrum of the MTM-SVD analysis of observed monthly SST variability over the Global Ocean from 40°S to 40°N from 1900 to 2000 [*Rayner et al.*, 2003] yields 6 peaks from 2- to 20-year periods that exceed the 99% confidence level (Figure 1a). Most of the spectrum for periods <2-year period is not displayed, but contains local fractional variance well below the 99% confidence level. Four peaks near ~2.9-year, ~3.5-year, ~4.2-year, and ~5.9-year period are classified as ENSO signals [e.g., *Allan*, 2000]. The other two spectral peaks correspond to the quasibiennial oscillation (QBO) centered near 2.1-year period and to the QDO centered near 11-year period. The frequencies of these QBO, ENSO, and QDO signals are consistent with those observed earlier in the joint MTM-SVD analysis of global SST and SLP variability over the late nineteenth and twentieth century [*Allan*, 2000; *White and Tourre*, 2003].

[19] Now we examine the MTM-SVD local fractional variance spectra of model monthly SST variability over the Global Ocean from 40°S to 40°N from the 350-year solar-forced FOAM simulation. We divide this simulation into three 100-year records, each representing one member of a three-member ensemble, and compute a spectrum for each member (Figures 1b-1d). The spectrum for each ensemble member exhibits a significant peak near 11-year period that corresponds to the model QDO, with the percentage of local fractional variance rivaling that of the model ENSO. This indicates that indeed some kind of ocean/atmosphere response to the radiative forcing by the 11-year signal in the Sun's total irradiance occurred in the FOAM. During each ensemble member, a significant peak also occurs for ENSO frequencies, centered near 3.1-year period for the first ensemble member (Figure 1b), near 3.6-year period for the second ensemble member (Figure 1c), and near 4.0-year period for the third ensemble member (Figure 1d). These model ENSO peaks are bracketed by those observed, ranging from 3- to 5-year period (Figure 1a).

[20] We now superimpose the MTM-SVD local fractional variance spectrum of the control FOAM simulation in the absence of the 11-year-period solar forcing (dashed curve in Figures 1b–1d). It is computed as the ensemble-average right across the 300-year simulation from model 50 years to 350 years. This spectrum does not display a significant QDO peak near 11-year period. However, it does simulate a weaker broadband ENSO from 2.9- to 4.5-year period and a QBO peak near 2.1-year period similar to those observed (Figure 1a). Thus we can conclude that the ENSO and QBO are intrinsic aspects of the FOAM climate variability, presumed stochastically forced in the absence of external solar forcing.

[21] We now display the time sequence of the real amplitudes of the complex SVD mode of SST variability associated with the model QDO from the second ensemble member (Figure 1e), comparing it with the time sequence of the 11-year-period signal in the Sun's total irradiance. During this ensemble member, and indeed the other two as well (not shown), the real amplitudes lag the peak 11-year-period signal in solar forcing by 33° to 100° of phase (i.e., ~1–3 years). Because the time sequence of real amplitudes modulates the real spatial pattern of the complex SVD at 0° phase in the corresponding spatial phase sequence (Figure 2a, right), this means that the peak in the 11-year-period solar forcing leads the peak warm SST phase of the model QDO in the eastern equatorial Pacific Ocean by the same phase difference (i.e., 33° to 100°). This phase lag overlaps that (i.e., 0° to 66°) observed in the analysis of SST variability associated with the observed QDO [*White et al.*, 1997, 1998].

4. Comparing Global SST Variability of the Model and Observed ENSO and QDO

[22] We compare the observed and model spatial phase sequences of the complex SVD mode of SST variability associated with the ENSO (Figure 2a) and the QDO (Figure 2b) revealed in the MTM-SVD analysis. These model spatial phase sequences display the average evolution over the second ensemble member (i.e., from 150 to 250 years in the 350-year simulation) of the solar-forced FOAM, while the observed phase sequences display the averaged evolution over the 100 years of the twentieth century from 1900 to 2000.

[23] The observed SST variability of the ENSO in the tropical Pacific Ocean (Figure 2a, left) develops a regional maximum along the equator off the west coast of South America, growing in intensity along the equator over the 1/4 cycle leading up to peak warm and cool phases at 0° and 180° phase, respectively, while variability in the tropical Indian Ocean develops a regional maximum along the equator off the east coast of Africa, growing in intensity and extending eastward over the same 1/4 cycle. A similar pattern and evolution is exhibited in the tropical Pacific and Indian oceans by the model ENSO (Figure 2a, right), but with peak warm and cool phases in the eastern equatorial Pacific Ocean at 0° and 180° phase, respectively, weaker than observed and extending farther to the west (to the maritime coast of Asia), encroaching on the cool SST variability observed in the western equatorial Pacific Ocean (Figure 2a, left). In the tropical Atlantic Ocean, SST variability in both model and observed ENSO develop regional maxima off the equator near 10°N and 20°S, peaking at the same time as peak SST variability in the Pacific and Indian oceans (i.e., at 0° and 180° phase).

[24] The observed SST variability of the QDO in the tropical Pacific Ocean is maximum during the peak warm and cool phases at 0° and 180° phase, respectively (Figure 2b,

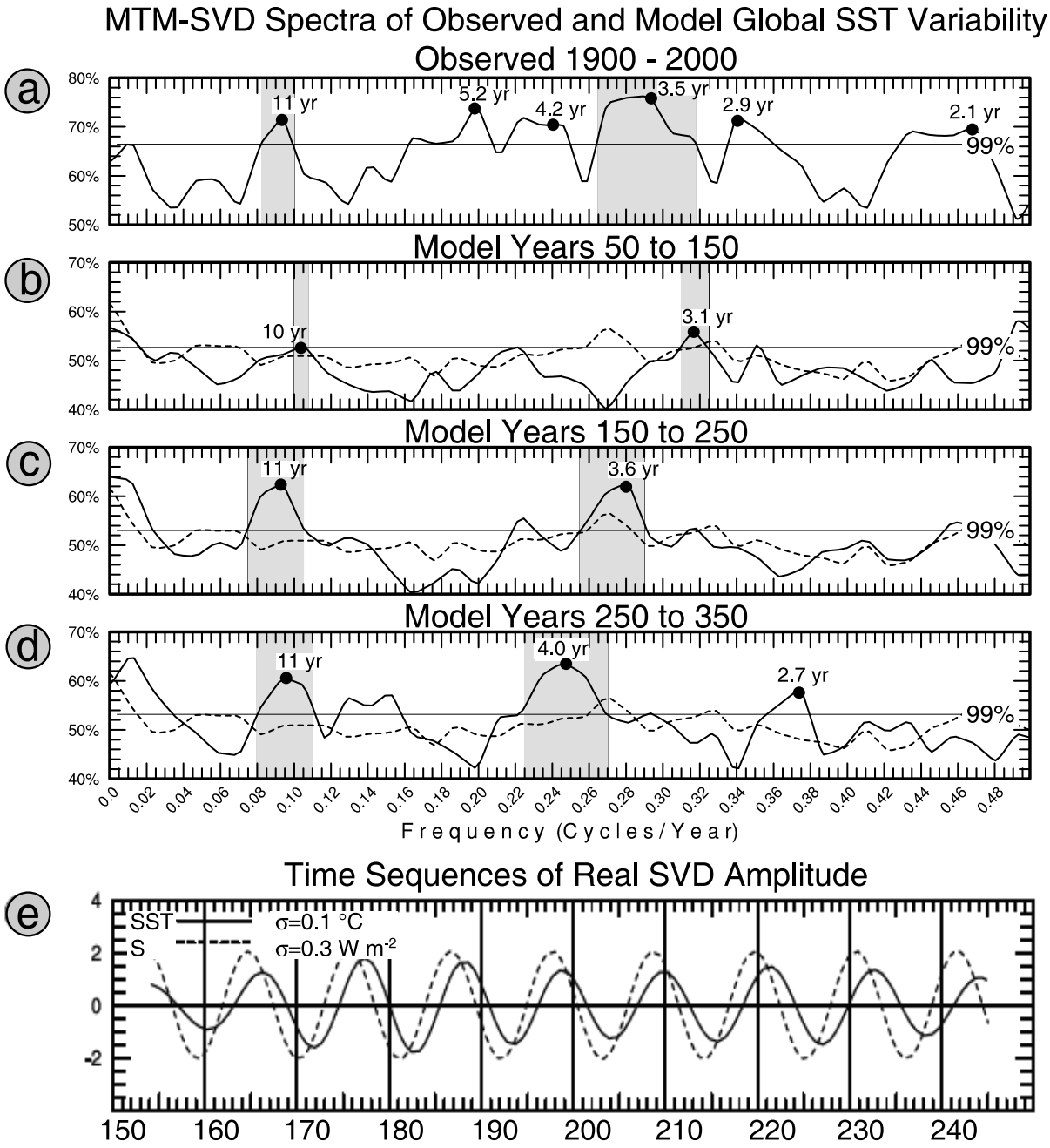

Figure 1. (a) MTM-SVD local fractional variance spectra of global SST variability observed over the global ocean (40°S to 40°N) from 1900 through 1999. (b, c, and d) Corresponding MTM-SVD spectra from the solar-forced FOAM simulation over the first ensemble member from 50 years to 150 years, the second ensemble member from 150 years to 250 years, and the third ensemble member from 250 years to 350 years. Superimposed on each of these FOAM spectra is the control model spectrum (i.e., in the absence of the 11-year-period solar forcing) averaged over the three ensemble members for the 300 years from 50 years to 350 years. The horizontal line indicates the 99% confidence level, above which the first complex SVD mode of variability in each frequency band must exceed in order to be considered significantly different from that achieved with random data. (e) The time sequence of the real amplitudes of the dominant complex SVD mode for the model QDO signal (i.e., for the second ensemble member from 150 years to 250 years), together with that of the idealized 11-year-period solar forcing. This amplitude time sequence modifies the spatial map of SST weights given at 0° phase in the corresponding phase sequence of the QDO (Figure 2b, right).

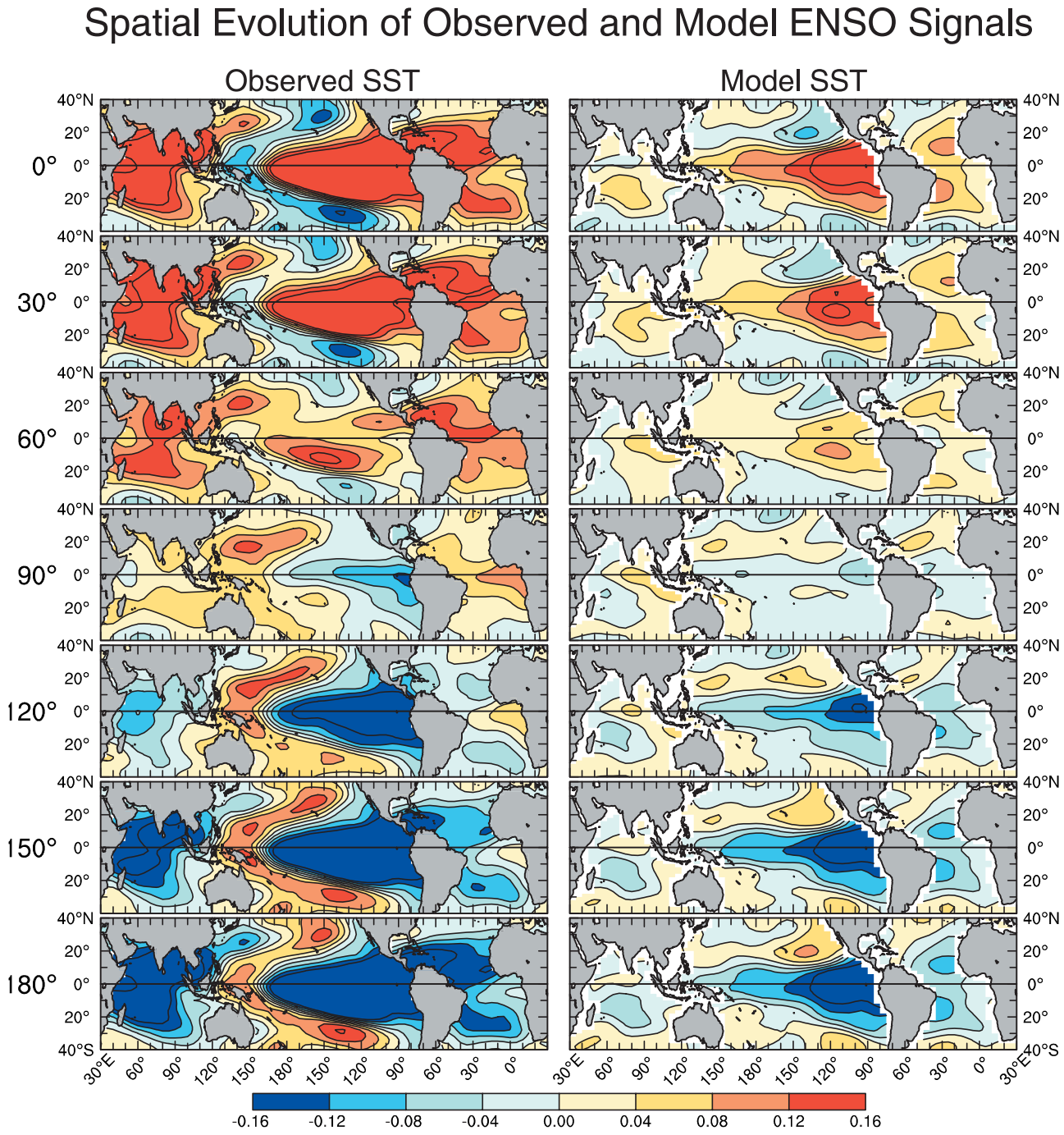

Figure 2a. Phase sequences of spatial maps of the first complex SVD mode for SST variability associated with ENSO of period 3 to 5 years, both (left) observed and (right) modeled with the solar-forced FOAM simulation, each phase sequence consisting of seven phase maps extending over 180° of phase (i.e., 1/2 cycle) in increments of 30° of phase and each map extending longitudinally around the globe from 40°S to 40°N. The sense of evolution comes from following weights of similar sign from one map to the next in each phase sequence. Yellow-to-red (blue) colors indicate warm (cool) SST weights. The color bar at the bottom ranges over ±0.16 standard deviations.

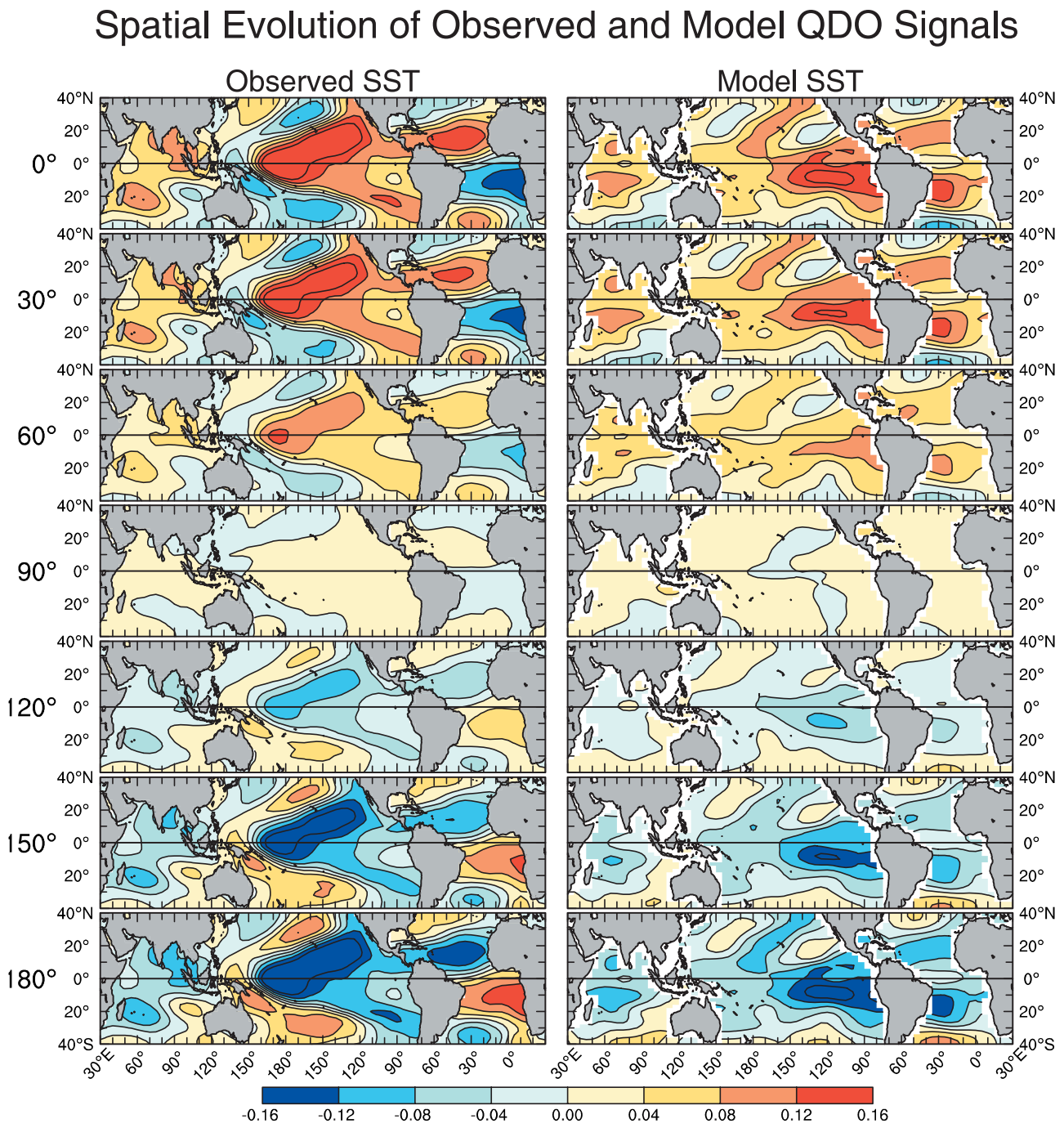

Figure 2b. The same as in Figure 2a, but for observed and model QDO of period 9 to 13 years.

left), manifested by a V-shaped standing wave pattern (i.e., on its side straddling the equator), with greater intensity in the tropical North Pacific Ocean than in the tropical South Pacific Ocean, and with an amplitude that intensifies over the 1/4 cycle leading up to peak warm and cool phases. In the tropical Indian Ocean, SST variability develops initially of the west coast of Australia in the South Indian Ocean and grows in intensity while propagating westward over the same 1/4 cycle. A similar pattern and evolution is exhibited in the tropical Pacific and Indian oceans by the model QDO (Figure 2b, right), though it displays greater intensity in the V-shaped standing wave pattern in the tropical South Pacific Ocean than in the tropical North Pacific Ocean; the V-shaped pattern also displaced farther to the west. In the tropical Atlantic Ocean, SST variability in the observed QDO (Figure 2b, left) develops a local maximum north of the equator near 12°N, out of phase with that near 12°S (i.e., the meridional dipole mode), peaking at the same time as SST variability in the tropical Pacific and Indian oceans. On the other hand, the model QDO in the tropical Atlantic

Ocean does not exhibit this meridional dipole structure (Figure 2b, right), with the sign of model SST variability in the tropical South Atlantic Ocean near 20°S the same as that in the tropical North Atlantic Ocean near 15°N. These hemispherical discrepancies between observed and model QDO's may be related to the mean state bias in the FOAM, which exhibits a double ITCZ across the entire global tropical Ocean [*Liu et al.*, 2004].

5. Covarying Model SST and SW Variability Over the Tropical Pacific Basin

[25] The tropical DAO mechanism shared by the observed ENSO and QDO in the Pacific Basin [*White et al.*, 2003b] depends on eastward ZSW anomalies within 10° latitude of the equator responding to and directed toward warm SST anomalies in the eastern/central equatorial Pacific Ocean during the peak warm phase. The poleward curvature of these eastward equatorial ZSW anomalies are associated with cyclonic WSC anomalies that drive the upwelling off-equatorial baroclinic Rossby waves responsible for the delayed negative feedback to equatorial SST anomalies [e.g., *Graham and White*, 1988]. These equatorial ZSW anomalies are in ageostrophic balance with SLP anomalies [*Ward and Hoskins*, 1996] arising from anomalous convection in the troposphere driven by underlying SST anomalies [*Graham and Barnett*, 1987]. Here we find this same equatorial ZSW response to SST anomalies in the model ENSO and QDO, revealed by the superposition of lag sequences of spatial maps of the dominant EEOF modes of SST and SW variability across the tropical Pacific Basin (Figure 3a).

[26] This superposition of lag sequences of the dominant SST and SW EEOF modes is allowed because corresponding amplitude time sequences, computed independently for each variable, fluctuate together on both period scales (Figure 3b). Utilizing these dominant modes is valid because the percentages of filtered SST (SW) variance over the 100-year record is 54% (39%) and 68% (53%) for the ENSO and QDO, respectively, significantly larger than (and independent of) the next most energetic modes of 9% (9%) and 9% (15%) [*North et al.*, 1982]. Moreover, the amplitude time sequence (Figure 3b) of the dominant EEOF SST mode of the QDO (with SST standard deviation of ~0.09°C) is comparable in magnitude to that of the ENSO (with SST standard deviation of ~0.10°C), as observed [*White et al.*, 2003b].

[27] The spatial phase relationships between model SST and SW variability in these EEOF lag sequences can be visualized in the last map (Figure 3a), which represents the warm phase of the model ENSO and QDO in the eastern/central tropical Pacific Ocean. These warm phases are characterized by warm SST weights straddling the equator, with maximum in the eastern tropical Pacific Ocean accompanied by eastward and southward SW weights straddling the western/central equatorial ocean on both period scales, as observed [*White et al.*, 2003b]. On ENSO (QOO) period scales, these eastward SW weights are directed toward warmest SST weights in the eastern equatorial Pacific Ocean (eastern tropical South Pacific Ocean near 10°S), as observed [*White et al.*, 2003b]. Off the equator, northward SW weights associated with the QDO in the tropical North Pacific Ocean are collocated with warm SST weights extending from the equator northeast through Hawaii (Figure 3a, right) as observed, presumably in Sverdrup balance with low-level atmospheric convergence variability arising from SST-induced deep convection [*White and Chen*, 2002; *White and Annis*, 2004].

[28] The spatial patterns of SST variability during the warm phase of the model ENSO and QDO (Figure 3a) display similarities and differences with each other and with those observed [*White et al.*, 2003b]. Both display the increase in meridional scale of equatorial SST and zonal SW weights with increasing period scale observed by *Tourre et al.* [2001], which is a necessary condition for driving off-equatorial Rossby waves farther off the equator with increasing period scale. On the other hand, the observed increase in longitude of maximum equatorial SST weights with increasing period scale [*Tourre et al.*, 2001] is missing in the FOAM, with the model SST pattern of both signals extending much farther to the west (indeed all across the equatorial Pacific Ocean) than that observed (Figure 2a, left). Even so, the model SW weights yield off-equatorial cyclonic WSC variability centered over the western and central tropical North Pacific Ocean near 10°N for the ENSO (Figure 3a, left) and near 20°N for the QDO (Figure 3a, right), the latter maximum from 160°E to 160°W, just west of Hawaii, as observed [*White et al.*, 2003b]. The resulting off-equatorial cyclonic WSC variability over the South Pacific Ocean for both model ENSO and QDO appear weaker than in the North Pacific Ocean, as observed for the ENSO but not for the QDO [*White et al.*, 2003b].

[29] The transition from cool phase to warm phase in the evolution of the model ENSO and QDO can be seen following SST weights of like sign from the third to sixth maps in the EEOF lag sequences (Figure 3a). Therein, the evolution of both signals has warm SST weights first appearing on the equator in the western ocean for the ENSO and in the central ocean for the QDO in the fourth map of each EEOF lag sequence, subsequently propagating eastward and reaching the west coast of South America by the fifth and sixth maps. This eastward phase propagation is consistent with the equatorial coupled waves observed by *White et al.* [2003b]. Also, in a conceptual model integrated by *White et al.* [2003b], these equatorial coupled waves were found providing a delay in the tropical DAO mechanism for the ENSO and QDO that was on the same order as the delay provided by the off-equatorial Rossby waves. This differs significantly from the original tropical DAO mechanism for ENSO [e.g., *Graham and White*, 1988], which depended on equatorial Kelvin waves conducting the signal across the Pacific Basin with comparably little delay compared to that of the off-equatorial Rossby waves.

6. Wind-Driven Off-Equatorial Rossby Waves

[30] Another component of the tropical DAO mechanism responsible for the observed ENSO and QDO [*White et al.*, 2003b] is the Ekman pumping of off-equatorial baroclinic Rossby waves from 5° to 25° latitude, which reflect at the maritime western boundary to produce a delayed negative feedback to SST variability in the eastern/central equatorial Pacific Ocean. This was first observed for the ENSO by *Graham and White* [1988] but not until much later for the

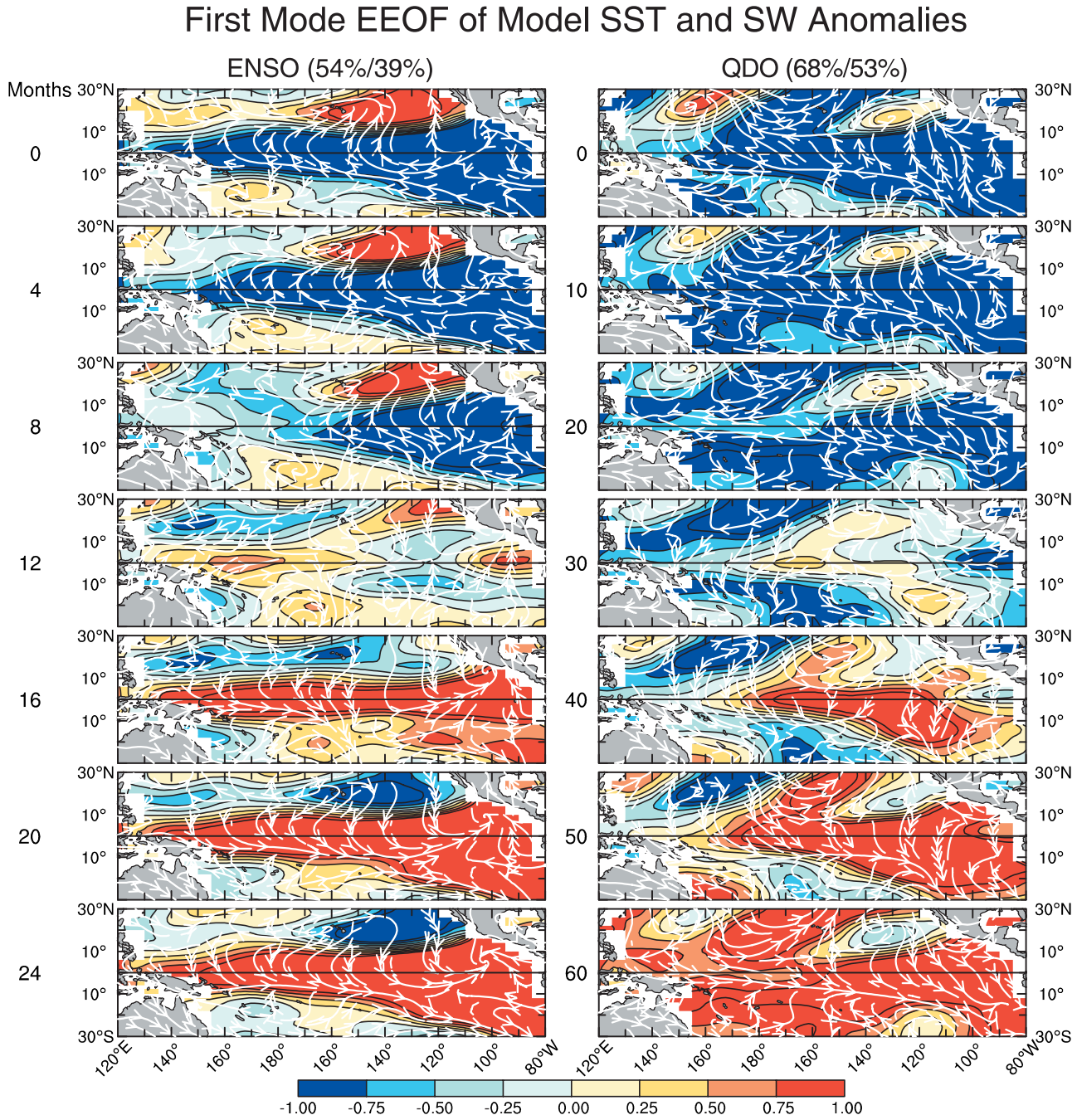

Figure 3a. Lag sequences of spatial maps of the dominant mode in the EEOF analysis of model SST and SW anomalies associated with (left) the ENSO and (right) the QDO in the solar-forced FOAM simulation, computed over the 100-year record of the second ensemble member. Each map extends over the Pacific Basin from 30°S to 30°N. Each lag sequence consists of seven maps extending from the tropical cool SST phase in the first lag map to the tropical warm SST phase in the seventh lag map, extending over one-half cycle of variability on each period scale (that is, ∼24 months and ∼60 months for the ENSO and QDO, respectively). The sense of propagation comes from following weights of similar sign or direction from one map to the next in each lag sequence. Yellow-to-red (blue) colors indicate warm (cool) SST weights; streamlines are parallel to SW weights. The color bar at the bottom ranges over ±1.0 standard deviations. Magnitude is given by the time sequences of amplitude (Figure 3b).

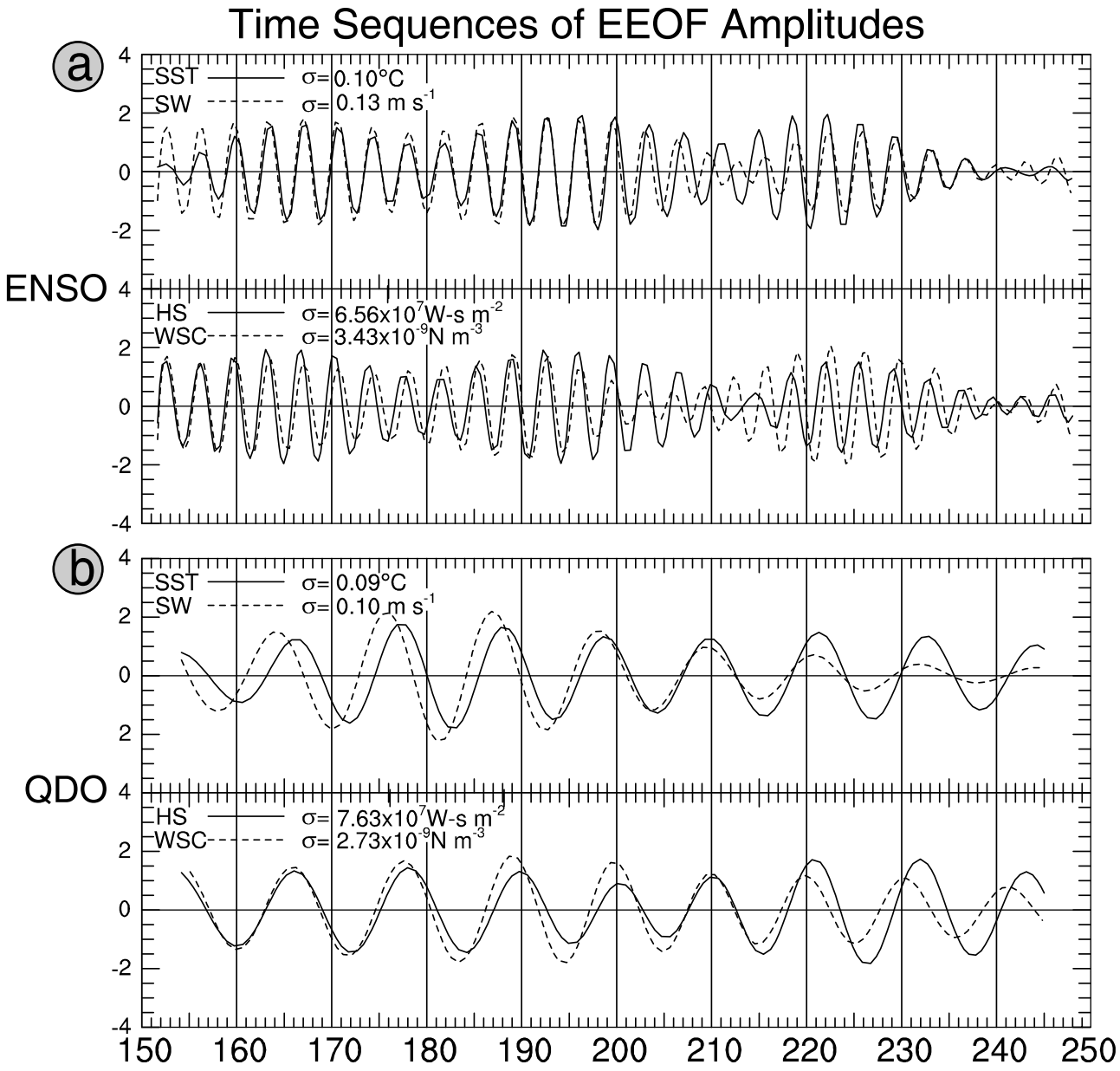

Figure 3b. Time sequences of amplitudes modulating the dominant lag sequences in the EEOF analysis of SST, SW, HS, and WSC anomalies over the second ensemble member from 150 years to 250 years of the solar-forced FOAM simulation associated with (a) the ENSO and (b) the QDO. Dominant EEOF modes account for 54%/39%/58%/32% and 68%/53%/55%/39% of the variance for SST/SW/HS/WSC anomalies associated with the ENSO and QDO, respectively. EEOF analysis was applied to SST, SW, HS, and WSC anomalies independently on each period scale. The ordinate gives the normalized amplitude of the signal, with the standard deviation (σ) given in each plot.

QDO [*White et al.*, 2003b]. Here we demonstrate this wind-driven off-equatorial Rossby wave activity in the FOAM by superimposing lag sequences of spatial maps of model HS and WSC variability from the first EEOF modes of model ENSO and QDO variability (Figure 3c). As with SST and SW lag sequences (Figure 3a), HS and WSC lag sequences can be superimposed because corresponding time sequences of amplitudes are aligned (Figure 3b). Moreover, they are aligned with those of SST and SW anomalies (Figure 3b), indicating that the entire baroclinic structure of the upper ocean and lower troposphere in the Pacific Basin fluctuate together in the FOAM on both period scales, as observed [*White et al.*, 2003b].

[31] The percentages of filtered variance explained over the 100-year record by these dominant HS (WSC) EEOF modes are 58% (32%) and 55% (39%) for the model ENSO and QDO, respectively, similar to those of dominant SST (SW) EEOF modes (Figure 3b). These percentages of filtered variance explained are significantly above those of the next most energetic modes of 8% (9%) and 16% (17%),

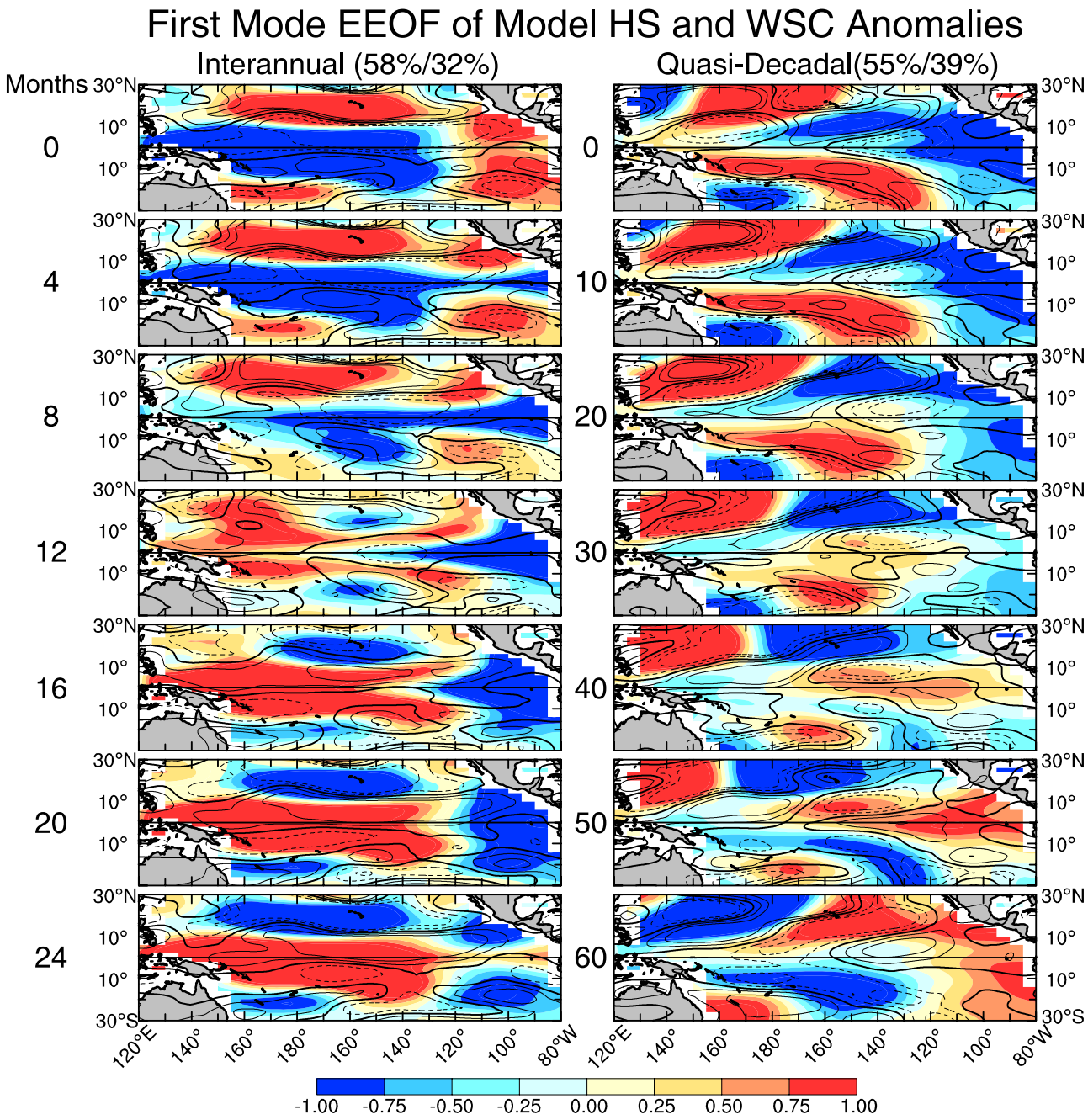

Figure 3c. Same as in Figure 3a, but for HS and WSC anomalies associated with (left) the ENSO and (right) the QDO in the solar-forced FOAM simulation. Each map extends over the Pacific Basin from 30°S to 30°N, with yellow-to-red (blue) colors indicating deep (shallow) HS weights and solid (dashed) contours indicating positive (negative) WSC weights. The color bar at the bottom ranges over ±1.0 standard deviations. The color contour interval of WSC weights is 0.25 standard deviations. Magnitude is given by the time sequences of amplitude (Figure 3b).

indicating that the first mode on each period scale displays negligible mixing with the next most energetic mode [*North et al.*, 1982].

[32] We begin our description of the wind-driven off-equatorial Rossby waves by following the evolution of interannual HS weights across the tropical North Pacific Ocean associated with the model ENSO (Figure 3c, left), where negative HS weights can be seen forming in the central tropical ocean just south of Hawaii from 10°N to 15°N in the fourth (i.e., center) map and subsequently spreading westward nearly to the maritime western boundary by the seventh (i.e., last) map in the lag sequence. Subsequently, we continue to follow the evolution of these negative HS weights by following the evolution of corresponding positive HS weights in the first map (i.e., similar to the last map but with the sign reversed), finding

them propagating westward while migrating equatorward to intersect the maritime western boundary near 5°N during the fourth (i.e., center) map, this evolution completing 1/2 cycle of ENSO variability.

[33] This evolutionary behavior shares similarities with that observed [*White et al.*, 2003b], wherein negative Z18 (depth of the 18°C isotherm) weights propagated westward across the tropical North Pacific Ocean from the eastern boundary from 10°N to 20°N to the western boundary from 5°N to 15°N over 1/2 cycle, with the wave amplitude intensifying dramatically under cyclonic WSC forcing across the central tropical North Pacific Ocean centered south of Hawaii from 5°N to 15°N; in the model, this is where the negative HS weights were initialized. Thus the model did not exhibit baroclinic Rossby waves emanating from the eastern boundary as part of the observed tropical DAO mechanism [*White et al.*, 2003b]. On the other hand, in both model and observed EEOF lag sequences, these upwelling baroclinic Rossby waves were either intensified (in the observations) or initialized (in the model) by cyclonic WSC weights (i.e., upwelling Ekman pumping) that extended zonally right across most of the tropical North Pacific Ocean from 10°N to 20°N during the cool phase of ENSO in maps 0–12 and from 0° to 15°N during the warm phase of ENSO in maps 16–24 (Figure 3c, left) in association with ZSW weights directed toward warm SST weights near the equator.

[34] Now we focus on the description of the wind-driven off-equatorial Rossby waves in the evolution of quasidecadal HS weights in the tropical North Pacific Ocean associated with the model QDO (Figure 3c, right). We find negative HS weights in the central tropical North Pacific Ocean from 10°N to 25°N (in the vicinity of Hawaii) in the fourth (i.e., center) map propagating directly westward to the maritime western boundary of Asia by the seventh (i.e., last) map in the lag sequence. Subsequently, we follow the evolution of these negative HS weights by following the evolution of corresponding positive HS weights in the first map (i.e., similar to the last map but with the sign reversed), finding them continuing to propagate directly westward to intersect the maritime western boundary from 5°N to 20°N by the second, third, and fourth maps, completing 1/2 cycle. Throughout this 1/2 cycle, cyclonic WSC weights in the central tropical North Pacific Ocean (in the vicinity of Hawaii) continues to pump this westward propagating baroclinic Rossby wave, with the cyclonic WSC weights propagating westward as well across the central and western tropical North Pacific Ocean during the last 1/4 cycle. This behavior also shares similarities with that observed [*White et al.*, 2003b], wherein negative HS weights propagated westward from the central tropical North Pacific Ocean from 10°N to 20°N (south of Hawaii) to the maritime western boundary over the corresponding 1/2 cycle, with amplitude intensifying dramatically across the central and western tropical North Pacific Ocean under continuous cyclonic WSC forcing (i.e., upwelling Ekman pumping) in the vicinity and west of Hawaii, with these WSC weights also propagating westward during the last 1/4 cycle as simulated in the model. The latter is indicative of coupled baroclinic Rossby wave activity [*White et al.*, 2003b], the phase speed of which was found to be ~1/2 that of uncoupled baroclinic Rossby waves [*Killworth et al.*, 1997].

[35] In the southern hemisphere, the generation of negative HS weights by negative cyclonic WSC weights associated with the model ENSO in the central/western tropical South Pacific Ocean during the last half of the EEOF lag sequence (Figure 3c, left) was much weaker than in the northern hemisphere and contributed little to reflection onto the equator over subsequent maps, as observed [*White et al.*, 2003a]. On the other hand, no generation of negative HS weights by cyclonic WSC weights could be found associated with the model QDO in the central/western tropical South Pacific Ocean in the fourth (i.e., center) map of the EEOF lag sequence (Figure 3c, right). However, in the seventh (i.e., last) map, negative HS weights were being driven in the central and western tropical South Pacific Ocean by negative cyclonic WSC weights. As we continue to follow the evolution of these negative HS weights by following the evolution of corresponding positive HS weights in the first map (i.e., similar to the last map but with the sign reversed), we find them reaching the maritime western boundary from 5°S to 10°S in the first and second maps, nearly as strong as simulated in the North Pacific Ocean. This evolution was different than observed [*White et al.*, 2003b], which found the evolution of the Rossby wave activity associated with the QDO in the tropical South Pacific Ocean to be nearly symmetric with that in the tropical North Pacific Ocean.

7. Western Boundary Reflection of Incident Off-Equatorial Baroclinic Rossby Waves

[36] We describe the western boundary reflection process of the off-equatorial baroclinic Rossby waves associated with the model ENSO and QDO by constructing time-distance diagrams around a circuit on each period scale in the North Pacific Ocean for 50 years from 200 years to 250 years in the second ensemble member of the solar-forced FOAM simulation (Figure 4). These two circuits follow the paths of off-equatorial Rossby waves westward across the tropical North Pacific Ocean from the eastern boundary to the maritime western boundary of Asia; then, they follow equatorial coupled waves eastward along on the equator and northward along the eastern boundary to the beginning of the circuit. That portion of the circuit off the equator is chosen by following the westward propagation of maximum HS weights across the tropical North Pacific Ocean from map to map in the EEOF lag sequence of spatial maps (Figure 3c). This exercise finds the most frequent incidence of off-equatorial Rossby waves on the western boundary for the ENSO and QDO to be near 5°N and 11°N, respectively. While the western boundary reflection process dominated the 50-year record (Figures 4a and 4b), it disappeared during significant portions of the record, as observed [*White et al.*, 2003b].

[37] For the ENSO, western boundary reflection occurred reliably over the first 15 years (i.e., 200 years to 215 years) and during the middle 10 years (i.e., 220 years to 230 years) of the 50-year record (Figure 4a), when westward propagating Rossby waves off the equator (from 50 to 145 scale distance along the path) propagated continuously into eastward propagating waves on the equator (from 145 to 300 scale distance along the path). Along this path, the off-

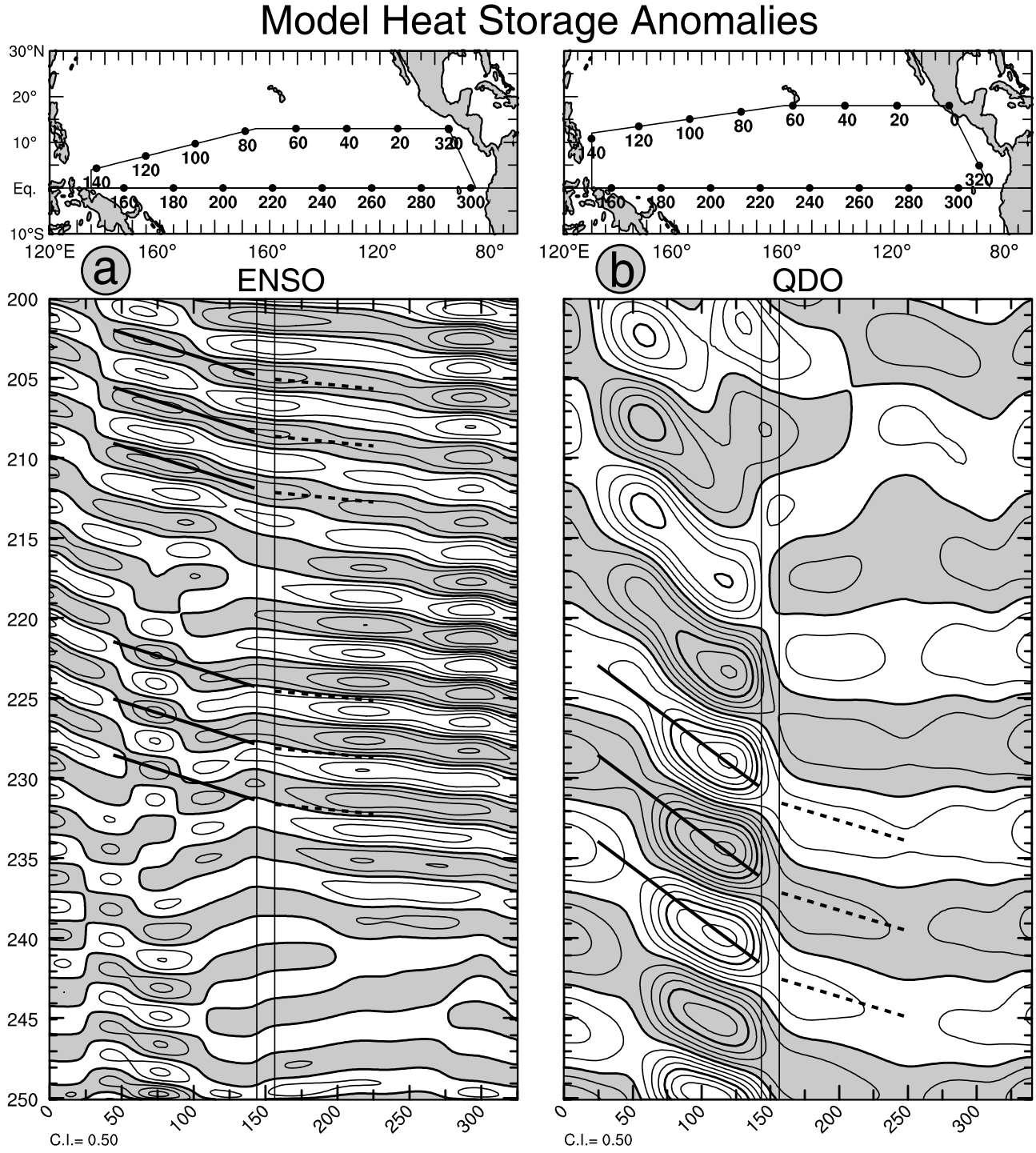

Figure 4. (top) Paths of the time-distance diagrams of model HS anomalies in the North Pacific Ocean associated with (bottom left) the ENSO and (bottom right) the QDO in the FOAM. (bottom) Time-distance diagrams of model HS anomalies extending along the aforementioned paths associated with (left) the ENSO and (right) the QDO for the 50 years from 200 years to 250 years in the 350-year integration of FOAM under the 11-year-period solar forcing. Negative (positive) anomalies are shaded (unshaded). Sloping black lines and sloping dashed lines highlight the continuity of westward propagating Rossby waves off the equator with eastward propagating coupled waves on the equator, respectively. Contour intervals are 5.0 m.

equatorial Rossby waves can be seen traveling slower on average (i.e., 0.15 to 0.25 m s^{-1}) than the equatorial coupled waves (i.e., 0.25 to 0.45 m s^{-1}), similar to corresponding observed phase speeds [*White et al.*, 2003b]. During the last 10 years of the 50-year record, the equatorial coupled waves on the equator propagated westward, while those off the equator continued to propagate westward as well. This change in wave direction is consistent with that observed in the evolution of the ENSO [*Wang*, 1995; *White and Cayan*, 2000; *White et al.*, 2003b; *White and Annis*, 2004], with equatorial coupled waves propagating eastward from 1966 to 1975 and westward from 1955 to 1966 (for example). In the latter case, the tropical DAO mechanism governing ENSO took a different form than that initially described [*Graham and White*, 1988] and simulated in 1.5 layer models [e.g., *Zebiak and Cane*, 1987; *Schopf and Suarez*, 1988], with the westward phase propagation of equatorial coupled waves linked to the eastern boundary reflection of eastward propagating ACW-like coupled waves in the tropical South Pacific Ocean incident on the west coast of northern Chile, Peru, and Ecuador [*White and Annis*, 2004]. It remains to be seen whether this kind of change in the tropical DAO mechanism occurs in the FOAM as well, it being beyond the scope of the present study.

[38] For the QDO, western boundary reflection occurred reliably over the last 30 years of the 50-year record (Figure 4b), with westward propagating baroclinic Rossby waves off the equator (from 0 to 150 scale distance along the path) propagating unbroken into eastward propagating waves on the equator (from 150 to 250 scale distance along the path), the Rossby waves traveling slower on average (i.e., 0.05 to 0.07 m s^{-1}) than the equatorial coupled waves (i.e., ~0.10 to 0.15 m s^{-1}), the latter confined to the western and central equatorial Pacific Ocean, similar to that observed [*White et al.*, 2003b]. During the first 15 years of the 50-year record, the QDO waves on the equator propagated westward, this change consistent with the evolution of the observed QDO [*White et al.*, 2003b], which displayed equatorial coupled waves propagating westward from 1955 to 1970 and eastward from 1970 to 1990 (for example). It remains to be seen in both the observations and in the solar-forced FOAM simulation whether this change in evolution is associated with a change in tropical DAO mechanism, as appears to be the case for the observed ENSO [*White and Annis*, 2004].

8. Discussion and Conclusions

[39] *White et al.* [2001] proposed that the tropical DAO mechanism governing the QDO of 9- to 13-year-period scale in the Pacific Basin was similar to that governing the ENSO of 3- to 5-year-period scale, but resonantly excited by the surface radiative forcing from the 11-year-period signal in the Sun's total irradiance. They tested this hypothesis by driving a conceptual ocean-atmosphere coupled model of the tropical DAO mechanism in the Pacific Basin with idealized 11-year-period solar forcing (i.e., cosine variability with realistic amplitude), this model having been used previously to simulate the spectrum of ENSO variability under stochastic forcing [*Graham and White*, 1988; *Graham et al.*, 1990]. This model experiment yielded a quasidecadal signal (i.e., the QDO) that rose significantly above the background spectrum of noise, rivaling the magnitude of the stochastically forced ENSO, and depending on a delayed negative feedback from baroclinic Rossby waves much farther poleward (i.e., between 12° and 18° latitude) as shown theoretically by *Graham et al.* [1990]. Because the amplitude of the model QDO was an order of magnitude larger than the Stefan-Boltzmann response, *White et al.* [2001] proposed that the QDO was in damped resonance with the 11-year period solar forcing. Subsequently, *White et al.* [2003b] described the tropical DAO mechanism governing the QDO in the Pacific basin, finding it similar to that governing the ENSO, as modeled by *Graham et al.* [1990] and *White et al.* [2001], that is, depending on the delayed negative feedback from off-equatorial Rossby waves between 10° and 20° latitude, but also depending on the delay of the eastward-propagating equatorial coupled waves from the western boundary to the central/eastern equatorial ocean.

[40] These foregoing observational and modeling studies set the stage for the present study in which we tested the damped resonance excitation hypothesis of the tropical DAO mechanism in a fully coupled ocean-atmosphere general circulation model (i.e., FOAM) by simply augmenting the mean radiative forcing by the Sun (i.e., the solar constant) with an 11-year-period signal (i.e., idealized by cosine variability), with amplitude that fluctuated ~0.1% about the mean as observed [*Lean et al.*, 1995a]. We found the control FOAM simulation, in the absence of the 11-year-period solar forcing, simulating an ENSO of 2.9- to 4.5-year period and a QBO of ~2.1-year period in response to stochastic forcing, but not the QDO of 9- to 13-year period. Earlier, *Liu et al.* [2000] had found the patterns and evolution of this model ENSO similar to those observed.

[41] On the other hand, the solar-forcing FOAM simulated all three signals (i.e., the QBO, ENSO, and QDO) in the upper ocean and lower atmosphere across the Pacific Basin. Here we demonstrated that the ENSO and QDO shared patterns and evolution similar to each other and to those of the tropical DAO mechanism governing the observed ENSO and QDO in the Pacific Ocean [*White et al.*, 2003b]. Furthermore, we found the warm SST phase of the model QDO in the eastern/central tropical Pacific Ocean lagging the 11-year-period solar forcing by 33° to 100° of phase, ovelapping that (i.e., 0° to 66°) observed [*White et al.*, 1997] and exhibiting an amplitude similar to that of ENSO as simulated in the conceptual tropical Pacific DAO model [*White et al.*, 2001]. This nominal amplitude and phase agreement allows us to conclude that the QDO in both the FOAM and the Earth's climate system arose as a damped resonant response of the tropical DAO mechanism to the 11-year-period solar forcing.

[42] In both the FOAM and the observations, the tropical DAO mechanism shared by the ENSO and QDO in the tropical Pacific Basin differed from one another not in component wave types, but in their speed of propagation; i.e., in the latitude and hence westward phase speed of off-equatorial baroclinic Rossby waves, and in the eastward phase speed of the equatorial coupled waves. Moreover, the model tropical DAO mechanism for the ENSO was stronger in the North Pacific Ocean than in the South Pacific Ocean, while that for the QDO was more symmetric about the

equator, as observed [*White et al.*, 2003b]. Thus off-equatorial Rossby waves in the FOAM were driven in the central tropical North Pacific Ocean by off-equatorial anomalous WSC forcing associated with equatorial SST-induced ZSW anomalies, the meridional scale of which increased with period scale, as proposed theoretically by *Graham et al.* [1990] and subsequently observed by *Tourre et al.* [2001]. Because the meridional scale of equatorial SST and ZSW anomalies increased with increasing period scale in both model and observations, the resulting anomalous WSC forcing of off-equatorial Rossby waves in the central tropical North Pacific Ocean occurred near 12°N for the ENSO (traveling westward at ~0.20 m s^{-1}) and near 18°N for the QDO (traveling westward at ~0.06 m s^{-1}). The tropical DAO mechanism also depended on the eastward phase speed of the equatorial coupled waves, which in both the observations and the FOAM were found propagating eastward across the equatorial Pacific Ocean faster for the ENSO (~0.30 m s^{-1}) than for the QDO (~0.10 m s^{-1}), both an order of magnitude slower than the phase speed of equatorial baroclinic Kelvin waves. This indicated that the eastward phase speeds of the equatorial coupled waves of the ENSO and QDO depend on different coupling thermodynamics [e.g., *Hirst*, 1986; *Neelin*, 1991; *Wang and Weisberg*, 1994], the thermodynamics of which have yet to be diagnosed.

[43] In spite of the general similarity in pattern and evolution of the simulated QDO with that observed, the model QDO exhibited some deficiencies. In the tropical Pacific Ocean, the tropical warm and cool phases of the QDO extended too far into the western equatorial Pacific, and were too intense south of the equator in the eastern/central tropical South Pacific Ocean. In the tropical Atlantic Ocean, the model QDO was symmetric about the equator, while that observed formed a dipole mode that has been recognized as the most dominant climate variability mode there [*Hastenrath*, 1984; *Houghton and Tourre*, 1992]. These latter deficiencies are likely related to the double ITCZ bias in the FOAM climatology [*Liu et al.*, 2004], which is a common bias for most coupled general circulation models [*Davey et al.*, 2002], while the extension of the model Cold Tongue into the western equatorial Pacific Ocean is likely responsible for the model QDO penetration there. Because the double ITCZ and Cold Tongue biases are a common bias of current coupled models, these deficiencies in the simulated QDO are likely to be exhibited in other climate models. This indicates a challenge for the simulation of the observed QDO in climate models.

[44] Finally, the present study suffers from FOAM being forced by idealized solar forcing composed of a pure cosine wave of 11-year period and uniform amplitude, while the real ~11-year-period signal in the Sun's irradiance is more broadband, with peak solar forcing during the twentieth century separated by 9 to 13 years and of variable amplitude [*Lean et al.*, 1995a]. It remains to be seen whether the proposed damped resonant excitation of the tropical DAO mechanism governing the QDO will be quite so efficacious under the more realistic, broadband, 11-year-period solar forcing. Furthermore, *White et al.* [2003a] and *White* [2006] found the tropical global-average temperature of the upper ocean (0.1°C) not driven by the ~11-year-period signal in surface solar radiative forcing, but rather indirectly (via variable sensible-plus-latent heat flux) by a greater warming of the tropical troposphere temperature (0.2°–0.5°C) in response to the ~11-year-period signal in the Sun's UV radiative forcing of the lower stratosphere temperature (~1.0°C) via absorption by ozone. Moreover, the latter was found modified by partial absorption of the Sun's and Earth's near-IR irradiance by variable volcanic aerosols, as proposed by *Labitzke and van Loon* [1995, 1997a, 1997b, 1999], *Robock* [2000], and others. Thus the next step in verifying the damped-resonance excitation hypothesis must include realistic monthly solar forcing across the Sun's irradiance spectrum, with the percentage variability (for example) of the UV component (2–3% of the mean) fluctuating more than an order of magnitude larger than that of the visible and IR components (~0.1% of the mean) [*Lean et al.*, 1995a, 1995b]. It must also include the realistic radiative forcing of the lower stratosphere and troposphere in response to variable volcanic aerosols.

[45] **Acknowledgments.** We would like to thank Yafang Zhong, who performed the FOAM simulation experiments and conducted preliminary analysis of the results. Appreciation is extended to Arthur (Ted) Walker, the programmer responsible for the analysis of FOAM results presented in this study. We extend our thanks to Andrea Fincham, who was responsible for drafting the figures displayed in this study. Warren White is supported by the National Aeronautics and Space Administration (NASA) under contract JPL1205106 and by the Scripps Institution of Oceanography at the University of California, San Diego. Zhengyu Liu is supported by NOAA and DOE.

References

Allan, R. J. (2000), ENSO and climatic variability in the last 150 years, in *El Niño and the Southern Oscillation: Multiscale Variability, Global and Regional Impacts*, edited by H. F. Diaz and V. Markgraf, pp. 3–35, Cambridge Univ. Press, Cambridge, U. K.

Allan, R. J., C. J. C. Reason, J. A. Lindesay, and T. J. Ansell (2003), 'Protracted' ENSO episodes and their impacts in the Indian Ocean region, *Deep Sea Res., Part II*, *50*, 2331–2347.

Capotondi, A., and M. A. Alexander (2001), Rossby waves in the tropical North Pacific and their role in decadal thermocline variability, *J. Phys. Oceanogr.*, *31*, 3496–3515.

Davey, M. K., et al. (2002), STOIC: A study of coupled model climatology and variability in tropical ocean regions, *Clim. Dyn.*, *18*, 403–420.

Douglass, D. H., and B. D. Clader (2002), Climate sensitivity of the Earth to solar irradiance, *Geophys. Res. Lett.*, *29*(16), 1786, doi:10.1029/2002GL015345.

Drake, J., I. Foster, J. Michalakes, B. Toonen, and P. Worley (1995), Design and performance of a scalable parallel community climate model, *Parallel Comput.*, *21*, 1571–1591.

Graham, N. E., and T. P. Barnett (1987), Sea surface temperature, surface wind divergence, and convection over tropical oceans, *Science*, *238*, 657–659.

Graham, N. E., and W. B. White (1988), The El Niño cycle: A natural oscillator of the Pacific ocean-atmosphere system, *Science*, *240*, 1293–1302.

Graham, N. E., W. B. White, and A. Pares-Sierra (1990), Low frequency ocean-atmosphere interactions in the tropical Pacific, in *Air-Sea Interaction in the Tropical Western Pacific*, edited by C. Jiping and J. Young, pp. 457–484, China Ocean Press, Beijing.

Hastenrath, S. (1984), Interannual variability and annual cycle: Mechanisms of circulation and climate in the tropical Atlantic sector, *Mon. Weather Rev.*, *112*, 1097–1107.

Hirst, A. C. (1986), Unstable and damped equatorial modes in simple coupled ocean-atmosphere models, *J. Atmos. Sci.*, *43*, 606–630.

Houghton, R. W., and Y. M. Tourre (1992), Characteristics of low-frequency sea surface temperature fluctuations in the tropical Atlantic, *J. Clim.*, *5*, 765–771.

Jacob, R., C. Schafer, I. Foster, M. Tobis, and J. Anderson (2001), Computational design and performance of the Fast Ocean-Atmosphere Model, version one, in *Proceedings of the 2001 International Conference on Computational Science*, edited by V. N. Alexandrov, J. J. Dongarra, and C. J. K. Tan, pp. 175–184, Springer, New York.

Kaylor, R. E. (1977), *Filtering and Decimation of Digital Time Series, Tech. Note BN 850*, Inst. for Phys. Sci. and Technol. Univ. of Md.,

College Park.
Killworth, P. D., D. B. Chelton, and R. A. de Zoeke (1997), The speed of observed and theoretical long extra-tropical planetary waves, *J. Phys. Oceanogr.*, *27*, 1946–1966.
Labitzke, K., and H. van Loon (1995), Connection between the troposphere and stratosphere on a decadal scale, *Tellus, Ser. A*, *47*, 275–286.
Labitzke, K., and H. van Loon (1997a), Total ozone and the 11-year sunspot cycle, *J. Atmos. Sol. Terr. Phys.*, *59*, 9–19.
Labitzke, K., and H. van Loon (1997b), The signal of the 11-year sunspot cycle in the upper troposphere-lower stratosphere, *Space Sci. Rev.*, *80*, 393–410.
Labitzke, K., and H. van Loon (1999), The Stratosphere, Phenomena, History, and Relevance, 179 pp., Springer, Berlin.
Lean, J. L., J. Beer, and R. Bradley (1995a), Reconstruction of solar irradiance since 1610: Implications for climate change, *Geophys. Res. Lett.*, *22*, 3195–3198.
Lean, J. L., O. R. White, and A. Skumanich (1995b), On the solar ultraviolet irradiance during the Maunder Minimum, *Global Biogeochem. Cycles*, *9*, 171–182.
Liu, Z., and H. Yang (2003), Extratropical control on tropical climate: Atmospheric bridge and oceanic tunnel, *Geophys. Res. Lett.*, *30*(5), 1230, doi:10.1029/2002GL016492.
Liu, Z., J. Kutzbach, and L. Wu (2000), Modeling climate shift of El Niño in the Holocene, *Geophys. Res. Lett.*, *27*, 2265–2268.
Liu, Z., B. Otto-Bliesner, J. Kutzbach, L. Li, and C. Shields (2003), Coupled climate simulation of the evolution of global monsoons in the Holocene, *J. Clim.*, *16*, 2472–2490.
Liu, Z., Q. Zhang, and L. Wu (2004), Remote impact on tropical Atlantic climate variability: Statistical assessment and dynamical assessment, *J. Clim.*, *17*, 1529–1549.
Mann, M. E., and J. Park (1999), Oscillatory spatio-temporal signal detection in climate studies: A multiple-taper spectral domain approach, *Adv. Geophys.*, *41*, 1–131.
Neelin, J. D. (1991), The slow sea surface temperature mode and the fast-wave limit: Analytical theory for tropical interannual oscillations and experiments in a hybrid coupled model, *J. Atmos. Sci.*, *48*, 584–606.
North, G. R., T. L. Bell, R. F. Cahalan, and F. G. Moeng (1982), Sampling errors in the estimation of empirical orthogonal functions, *Mon. Weather Rev.*, *110*, 699–706.
Philander, S. G. H. (1990), *El Nino, La Nina, and the Southern Oscillation*, 293 pp., Academic Press, San Diego, Calif.
Rayner, N. A., D. E. Parker, E. B. Horton, C. K. Folland, L. V. Alexander, D. P. Rowell, E. C. Kent, and A. Kaplan (2003), Global analyses of sea surface temperature, sea ice, and night marine air temperature since the late nineteenth century, *J. Geophys. Res.*, *108*(D14), 4407, doi:10.1029/2002JD002670.
Reid, G. C. (1991), Solar total irradiance variations and the global sea surface temperature record, *J. Geophys. Res.*, *96*, 2835–2844.
Robock, A. (2000), Volcanic eruptions and climate, *Rev. Geophys.*, *38*, 191–219.
Schopf, P. S., and M. J. Suarez (1988), Vacillations in a coupled ocean-atmosphere model, *J. Atmos. Sci.*, *45*, 549–566.
Snedecor, G. W., and W. G. Cochran (1980), *Statistical Methods*, 507 pp., Iowa State Univ. Press, Ames, Iowa.
Tourre, Y. M., B. Rajagopalan, Y. Kushnir, M. Barlow, and W. B. White (2001), Patterns of coherent decadal and interdecadal climate signals in the Pacific Basin during the 20th century, *Geophys. Res. Lett.*, *28*, 2069–2072.
Wang, B. (1995), Interdecadal changes in El Niño onset in the last four decades, *J. Clim.*, *8*, 267–285.
Wang, C., and R. H. Weisberg (1994), On the "Slow Mode" mechanism in ENSO-related coupled ocean-atmosphere models, *J. Clim.*, *7*, 1657–1667.
Ward, M. N., and B. J. Hoskins (1996), Near surface winds over the global ocean 1949–1988, *J. Clim.*, *9*, 1877–1895.
Weare, B., and J. Nasstrom (1982), Examples of extended empirical orthogonal function analysis, *Mon. Weather Rev.*, *110*, 481–485.
White, W. B. (2006), Response of tropical global ocean temperature to the Sun's quasi-decadal UV radiative forcing of the stratosphere, *J. Geophys. Res.*, *111*, C09020, doi:10.1029/2004JC002552.
White, W. B., and J. Annis (2004), The influence of the Antarctic circumpolar wave on El Niño from 1950 through 2001, *J. Geophys. Res.*, *109*, C06019, doi:10.1029/2002JC001666.
White, W. B., and D. R. Cayan (2000), A global ENSO wave in surface temperature and pressure and its interdecadal modulation from 1900 to 1997, *Geophys. Res.*, *105*, 11,223–11,242.
White, W. B., and S.-C. Chen (2002), Thermodynamic mechanisms responsible for the troposphere response to SST anomalies in the Antarctic circumpolar wave, *J. Clim.*, *15*, 2577–2596.
White, W. B., and Y. M. Tourre (2003), Global SST/SLP waves during the 20th century, *Geophys. Res. Lett.*, *30*(12), 1651, doi:10.1029/2003GL017055.
White, W. B., J. Lean, D. R. Cayan, and M. Dettinger (1997), A response of global upper ocean temperature to changing solar irradiance, *J. Geophys. Res.*, *102*, 3255–3266.
White, W. B., D. R. Cayan, and J. Lean (1998), Global upper ocean heat storage response to radiative forcing from changing solar irradiance and increasing greenhouse gas/aerosol concentrations, *J. Geophys. Res.*, *103*, 21,355–21,366.
White, W. B., M. D. Dettinger, and D. R. Cayan (2001), Global average upper-ocean temperature response to changing solar irradiance: Exciting the internal decadal mode, in *SOLSPA 2000*: *Proceedings of the* 1st *Solar Space Weather,* edited by A. Wilson, *Eur. Space Agency Spec. Publ.*, *SP-463*, 125–133.
White, W. B., M. D. Dettinger, and D. R. Cayan (2003a), Sources of global warming in the upper-ocean on decadal period scales, *J. Geophys. Res.*, *108*(C8), 3248, doi:10.1029/2002JC001396.
White, W. B., Y. M. Tourre, M. Barlow, and M. Dettinger (2003b), A delayed action oscillator shared by biennial, interannual, and decadal signals in the Pacific basin, *J. Geophys. Res.*, *108*(C3), 3070, doi:10.1029/2002JC001490.
Wu, L., and Z. Liu (2005), North Atlantic decadal variability: Air-sea coupling, oceanic memory, and potential Northern Hemisphere resonance, *J. Clim.*, *18*, 331–349.
Wu, L., Z. Liu, R. Gallimore, R. Jacob, D. Lee, and Y. Zhong (2003), A coupled modeling study of Pacific decadal variability: The Tropical Mode and The North Pacific Mode, *J. Clim.*, *16*, 1101–1120.
Zebiak, S. E., and M. A. Cane (1987), Model El Niño-Southern Oscillation, *Mon. Weather Rev.*, *115*, 2262–2278.
Zhong, Y. (2004), Coupled response of global climate to solar forcing cycles, *CCR Contrib. 917*, Univ. of Wis., Madison.

Z. Liu, Center for Climate Research, Gaylord Nelson Institute for Environmental Studies, University of Wisconsin-Madison, Madison, WI 53706-1695, USA.

W. B. White, Scripps Institution of Oceanography, University of California, San Diego, La Jolla, CA 92037, USA. (wbwhite@ucsd.edu)